Energy Engineering

Tech Science Press

https://doi.org/10.32604/ee.2026.079956

ARTICLE

Two-Stage Optimization Strategy of EHDT-BSS Participating in Grid Frequency Regulation

Xin Li, Shuang Shi*, Qiyi Liu and Yan Zhang

State Grid Sichuan Electric Power Company Marketing Service Center (Metrology Center), Chengdu, China

*Corresponding Author: Shuang Shi. Email: shuangshi_sgcc_sc@126.com

Received: 31 January 2026; Accepted: 01 April 2026; Published: 18 June 2026

ABSTRACT: Electric heavy-duty truck battery swapping stations (EHDT-BSS) are emerging as flexible resources for power systems due to their high controllability and significant power capacity. However, the participation of EHDT-BSSs in grid frequency regulation is severely constrained by the limited battery quantity and the high stochasticity of swapping demand, where forecasting errors can affect system reliability. To address these challenges, this paper proposes a two-stage optimization strategy for EHDT-BSSs participating in frequency regulation considering demand uncertainty. First, the basic operation mode of BSS is designed, and a deep learning-based method is utilized to forecast swapping demand. A state-of-charge (SOC)-based battery classification mechanism is then established to ensure inter-temporal battery availability. The proposed framework includes a day-ahead scheduling stage to maximize the total revenue from frequency regulation and swapping services, followed by an intraday rolling optimization stage designed to compensate for real-time forecasting deviations. The results demonstrate that the proposed method effectively balances economic efficiency and operational reliability, enabling EHDT-BSSs to provide stable ancillary services while meeting heavy-duty truck swapping needs.

KEYWORDS: Battery swapping station; frequency regulation; two-stage optimization

1 Introduction

With the steady advancement of the global energy transition and the pursuit of "carbon peak and carbon neutrality" goals [1], vehicle electrification is accelerating [2]. Heavy-duty trucks (HDT), as a primary source of carbon emissions in the transportation sector, play a crucial role in this transformation [3]. Battery swapping has emerged as a crucial method for replenishing energy, offering distinct advantages in efficiency, speed, and safety [4–7]. Currently, Battery-swappable electric heavy-duty trucks (EHDT) are gaining significant market traction, paralleled by the large-scale construction of battery swapping stations [8–10]. EHDT battery swapping stations (EHDT-BSS) are characterized by high power demand and high controllability, positioning them as high-quality flexible resources [3]. Therefore, optimizing their charging and discharging behavior is essential for enhancing power system stability and reducing operational costs [11].

Extensive research has been conducted on the scheduling strategies for battery swapping stations (BSS). Early research primarily focused on orderly charging management of BSS by optimizing the number of batteries charged or the charging power, aiming to reduce operating costs and mitigate the impact on the power grid. Reference [12] treated individual battery packs as decision units and directly optimized the charging power of each battery in different time periods, enabling fine-grained power control. Reference [13]

constructed orderly charging models for electric vehicle battery swapping stations based on queueing theory, and by regulating the number of batteries put into charging in each time period, effectively reduced grid load fluctuations. Reference [14] adopted a SOC grading approach, in which batteries were classified into different SOC levels, and the charging quantities of each level were optimized. Reference [15] established a battery redundancy model under orderly charging conditions and optimized it using an adaptive genetic algorithm, which not only effectively reduced the peak-to-valley difference of grid load but also increased battery redundancy. Reference [16] proposed a charging decision model for BSS based on a variable population evolutionary algorithm. By optimizing the charging scheme to maximize battery inventory while minimizing charging losses, the model improves the operational efficiency and economic benefits of the station. Although previous studies have improved the orderly charging capability of BSS, they typically model BSS as pure charging loads and fail to fully exploit their charge–discharge flexibility.

With the development of Vehicle-to-Grid (V2G) technology, battery swapping stations, as distributed energy storage units with substantial controllable potential, have increasingly demonstrated their flexibility value to the power grid. Reference [17] proposed a dual-layer model predictive control (MPC) strategy to achieve coordinated control between the battery load demand of electric vehicle swapping stations and grid-side supply matching. Furthermore, Reference [18] investigated an intelligent peak-cutting and valley-filling charging and swapping mode based on potential game theory, which effectively optimizes the interaction between the swapping stations and the power grid. Reference [19] constructed an optimization model for photovoltaic battery swapping stations by integrating weather and traffic forecasts, achieving peak–valley regulation while ensuring battery swap demand, thereby effectively promoting renewable energy utilization and economic operation of the system. Moreover, as comprehensively reviewed in [20], BSSs are identified as grid-side distributed energy storage units and are shown to play a key role in power dispatch, peak–valley regulation, and ancillary services.

Regarding ancillary services, the inherent fast-response capability and power regulation of vehicle batteries have positioned BSS as a research focus for grid frequency regulation. The aggregated battery resources of swap stations can respond to Automatic Generation Control (AGC) signals within milliseconds, significantly outperforming the frequency response of conventional generators. Reference [21] proposed an optimal frequency regulation participation strategy for BSS considering uncertainties in swapping demand and regulation signals. A day-ahead bidding and real-time dispatch framework based on information-gap decision theory is adopted to improve profitability while maintaining regulation performance. Reference [22] introduced a deep Q-network-based scheduling strategy that enables swap stations to dynamically optimize their frequency regulation capacity and participate in fast frequency response services, thereby enhancing both economic benefits and regulation performance in the ancillary service market. Reference [23] further developed a secondary frequency control strategy for swap stations that accounts for user behavior and battery heterogeneity; using a distributed control approach, it stabilizes grid frequency while coordinating intra-station battery energy balance and health management. These studies indicate that, through advanced control and scheduling strategies, battery swapping stations can effectively serve as frequency regulation resources while ensuring the fulfillment of battery swap demand.

However, the aforementioned studies largely assume scenarios with sufficient in-station batteries or accurately predictable swap demand [21,22], and they often treat the swapping demand as a flexible soft constraint. In the case of EHTD-BSS, the limited number of batteries and the high randomness of swap demand make precise demand forecasting challenging, and forecasting errors can significantly impact

scheduling decisions. This renders traditional aggregated energy models or static scheduling methods less applicable [14]. Therefore, the uncertainties of swap demand in BSS should be considered when participating in grid frequency regulation. To address this, this study proposes a two-stage optimization framework for EHDT-BSS that explicitly considers forecast errors. First, the operational characteristics of the EHDT-BSS are modeled, integrated with a deep learning-based method to predict swapping demand. Subsequently, a day-ahead scheduling model is established to maximize the total revenue from both frequency regulation and swapping services based on forecasted demand. In the intraday operation, a real-time rolling optimization method is proposed to eliminate the effect of uncertainties of the swapping demand. The main contributions of this research are:

1. A basic operation mode of BSS is designed, including the battery classification method with a forecasting method of swapping demand. To ensure the demand for EHDT, a battery dispatch strategy for the current and next time period is proposed.
2. A two-stage optimization method of EHDT-BSS participating in grid frequency regulation is proposed. The day-ahead optimization method can help BSS reach the maximum benefits from the grid frequency regulation and meet the swapping demand of EHDT. Then, the effect of swapping demand uncertainties is solved by the rolling optimization in the intra-day operation. This two-stage structure effectively reaches a balance between economy and reliability under demand uncertainty.

The rest of this paper is organized as follows. Section 2 describes the operation mode of EHDT-BSS, including the forecasting method of swapping demand and battery dispatch plan in BSS; in Section 3, the two-stage optimization method is proposed; in Section 4, the case study is illustrated to verify the proposed method in Section 5.

2 Operation Model of BSS

2.1 Basic Operation Mode of BSS

A typical EHDT battery swapping station is a highly automated integrated system for safe and efficient battery replacement and charging. As shown in Fig. 1, the system primarily consists of a monitoring and control center, a swapping work bay, a battery swapping robot system, and a battery charging compartment. Specifically, the battery charging compartment is equipped with several regular charging slots. One transit charging slot is used for temporary battery storage, and another one serves as a backup charging slot for storing a spare battery. Externally, a transformer is provided exclusively to power the charging compartment. To ensure the continuity of the swapping process, this paper assumes that the number of batteries equipped in the station matches the number of regular charging slots.

The complete battery swapping process operates as follows: An EHDT enters the designated swapping work bay to initiate identity authentication. Subsequently, under the unified scheduling and safety monitoring of the station control system, the swapping robot unloads the depleted battery from the vehicle and transfers it to the transit charging slot. Next, a fully charged battery is selected from the regular charging slots and installed into the vehicle's battery compartment. Upon completion of the battery replacement, the vehicle exits the bay, and the swapping process ends. At this stage, the control system determines the charging strategy for the depleted battery temporarily stored in the transit charging slot. This entire sequence establishes an orderly "Unload-Transit-Load" workflow.

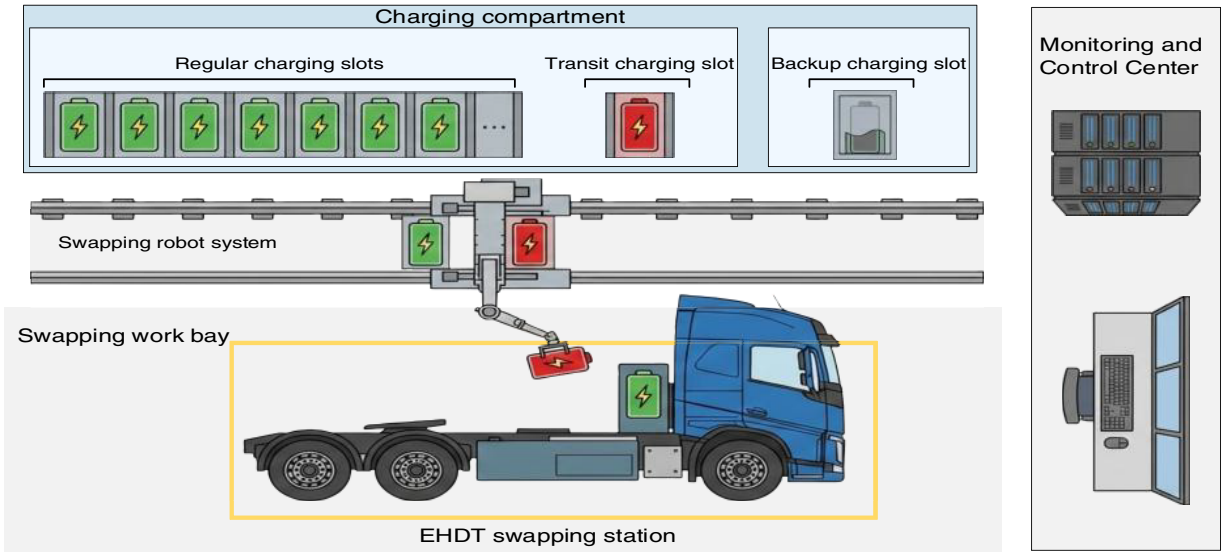

Figure 1: Structure diagram of the EHDT battery swapping station.

2.2 Battery Classification and Swap Demand Prediction

2.2.1 Battery Classification Method of BSS

The scheduling of EHDT-BSS fundamentally relies on the coordinated charging and discharging of on-site battery resources. However, distinct from standard passenger vehicle stations, EHDT-BSS facilities operate with a limited battery inventory and exhibit a tight coupling between swapping and charging processes. Consequently, battery availability fluctuates dynamically, driven by variations in charging protocols and swapping demand. To address these constraints, we propose a classification strategy based on SOC grading. In contrast to the static grading [14] or the highly discretized multi-energy-level division of batteries [11], the complex battery states are specifically classified into the following three SOC categories in this study. By categorizing and scheduling battery packs according to distinct grades, a robust mapping relationship is established between battery status and charging/discharging protocols. To facilitate the analysis of the scheduling optimization, the following assumptions are made:

1. All battery packs deployed in the battery swapping station are assumed to have uniform specifications and to operate under constant-power charging and discharging.
2. Battery packs removed during swapping are assumed to be immediately available for charging, subject to operational decisions.
3. To preserve battery longevity, a multi-stage charging and discharging strategy is adopted, with predefined thresholds imposed to prevent overcharging and deep discharging.

Let $SOC_{i,t}$ denote the state of charge of the i-th battery pack within the station at a discrete time step t. In line with the operational characteristics of BSS, the following SOC thresholds are defined: SOC_{min} represents the minimum safety limit for battery operation; SOC_{low} denotes the lower bound at which a battery retains flexible regulation capability; and SOC_{high} indicates the minimum SOC required for deployment in EHDT swapping. Based on these thresholds, the station's battery inventory is classified into three distinct SOC grades, denoted as S_1, S_2, and S_3, in descending order of charge level:

(a) Category 1: Fully Charged Reserve Batteries. This category represents the highest SOC range. Batteries in this classification satisfy the requisite criteria for swapping operations and are immediately deployable without the need for supplementary charging. Functioning as the core service resource of the BSS, this inventory is dedicated strictly to guaranteeing baseline swapping demands across all operational intervals. Consequently, under nominal conditions, these batteries are withheld from participating in grid discharge. The quantity of batteries in this category is denoted by N_{f}, and the corresponding set is defined as follows:

$$\Omega_{\mathrm{f},t} = \left\{ i \left| \mathrm{SOC}_{i,t} \geq \mathrm{SOC}_{\mathrm{high}} \right. \right\} \tag{1}$$

where: $\Omega_{\mathrm{f},t}$ represents the set of Category 1 batteries at time t; $\mathrm{SOC}_{i,t}$ represents the SOC value of the i-th battery at time t.

(b) Category 2: Flexible Regulation Batteries. This category comprises batteries whose SOC falls within the medium range. These batteries are capable of not only addressing extreme swapping demands in the next time period but also serving as the core flexible resource for the BSS to participate in grid frequency regulation services, possessing bidirectional charging and discharging capabilities. When current swapping demands are sufficiently covered by the quantity of Category 1 batteries, frequency regulation services can be provided by this category of batteries in response to under-frequency and over-frequency events in the power grid by following AGC commands. The quantity of batteries in this category is denoted by N_{d}, and the corresponding set is defined as:

$$\Omega_{\mathrm{d},t} = \left\{ i \left| \mathrm{SOC}_{\mathrm{low}} \leq \mathrm{SOC}_{i,t} < \mathrm{SOC}_{\mathrm{high}} \right. \right\} \tag{2}$$

where: $\Omega_{\mathrm{d},t}$ represents the set of Category 2 batteries at time t.

(c) Category 3: Discharged Batteries. Batteries that have just been swapped out from vehicles or discharged to the threshold are classified into this category. These batteries lack discharging capability and primarily respond to subsequent frequency regulation or swapping services by controlling their charging behavior. The quantity of batteries in this category is denoted by N_{c}, and the corresponding set is defined as:

$$\Omega_{\mathrm{c},t} = \left\{ i \left| \mathrm{SOC}_{\mathrm{min}} \leq \mathrm{SOC}_{i,t} < \mathrm{SOC}_{\mathrm{low}} \right. \right\} \tag{3}$$

where: $\Omega_{\mathrm{c},t}$ represents the set of Category 3 batteries at time t.

The charging power of the BSS at each time period is expressed as:

$$\begin{cases} P_{\mathrm{BSS},t} = P_{\mathrm{rigid},t} + P_{\mathrm{flex},t} \\ P_{\mathrm{rigid},t} = \sum\limits_{i \in \Omega_{\mathrm{c},t}} P_{\mathrm{ch},i,t} \\ P_{\mathrm{flex},t} = \sum\limits_{i \in \Omega_{\mathrm{d},t}} \left(P_{\mathrm{ch},i,t} - P_{\mathrm{dis},i,t} \right) \end{cases} \tag{4}$$

where: $P_{\mathrm{BSS},t}$ represents the charging power of the battery swapping station during time period t; $P_{\mathrm{rigid},t}$ denotes the rigid charging power, generated by the depleted battery set; $P_{\mathrm{flex},t}$ represents the flexible charging/discharging power, contributed by the flexible regulation batteries; $P_{\mathrm{ch},i,t}$ and $P_{\mathrm{dis},i,t}$ denote the charging and discharging power of the i-th battery during time period t, respectively.

2.2.2 Demand Forecasting Model for BSS

Compared with normal battery-swapping electric vehicles (EVs), the load of EHDTs exhibits distinct characteristics, specifically concentrated temporal distribution and high-power demand. On the one hand, constrained by the strict timeliness requirements of logistics tasks, battery-swapping demand often surges during specific shift handover periods, resulting in significant peak loads. On the other hand, although the operation schedules of EHDTs are relatively fixed, their transportation tasks are subject to the coupled influence of complex factors such as order dynamics, traffic conditions, and weather. Consequently, their battery-swapping behavior exhibits significant non-linearity and time-varying uncertainty, making it difficult for traditional linear prediction methods to capture the underlying deep dynamic patterns. Therefore, this paper proposes a stacked Long Short-Term Memory (LSTM) prediction model integrated with an attention mechanism [24]. This model utilizes historical operation data to accurately predict battery-swapping demand for future time intervals.

To ensure that the temporal resolution of the prediction model aligns with the physical operational characteristics of the BSS, this paper first defines the prediction time step. The model discretizes the 24-h day into T equal-length intervals. To achieve temporal consistency in the operation scheduling of the BSS, the time intervals are segmented based on battery charging characteristics. The interval step size, denoted as t_{p} (in minutes), is calculated according to Eq. (5):

$$t_{\mathrm{p}} = \frac{W_{\mathrm{B}}}{P_{\mathrm{ce}}} \times 60 \tag{5}$$

where: W_{B} denotes the rated capacity of the battery; P_{ce} represents the rated charging power of the battery swapping station. The day is discretized into multiple equal-length time intervals starting from 00:00. If the final interval of the current day is shorter than a complete time step t_{p}, it is completed using time from the subsequent day.

On this basis, a multi-dimensional feature matrix is constructed as the model input. Given the significant periodicity and regularity exhibited by the battery-swapping demand of electric heavy-duty trucks, the input features are primarily composed of historical battery-swapping order sequences and multi-dimensional temporal features. Specific time-step information is included in the temporal features, and workdays and non-workdays are also explicitly distinguished. After being standardized, the operational and scheduling patterns of electric heavy-duty trucks across different day types and time periods can be effectively reflected by these multi-dimensional features, whereby rich contextual information is provided for the model to capture deep dynamic time-series patterns.

The backbone of the prediction model adopts a stacked LSTM structure to hierarchically extract the temporal features of battery-swapping demand. The lower-layer LSTM captures short-term intraday fluctuation characteristics, while the upper-layer LSTM focuses on learning long-term inter-day patterns. Furthermore, considering the peak load characteristics of EHDT battery-swapping demand, this paper incorporates an attention mechanism at the LSTM output layer. This mechanism performs adaptive weighting on the hidden state sequence $H = \{h_1, h_2, \ldots, h_L\}$ output by the LSTM, enabling the model to focus on the historical time steps that are most relevant to the current prediction time t. At time t, for the i-th historical hidden state h_i, its normalized weight coefficient $\alpha_{t,i}$ is calculated via the Softmax function:

$$\alpha_{t,i} = \frac{\exp\left(\mathrm{score}\left(h_t, h_i\right)\right)}{\sum_{j=1}^{L} \exp\left(\mathrm{score}\left(h_t, h_j\right)\right)} \tag{6}$$

where: L denotes the length of the input time window; score $(\cdot)$ represents a correlation scoring function used to evaluate the significance of the hidden state h_i at historical time step i regarding the prediction result at the current time step t; h_t represents the LSTM hidden state at the current prediction time t; h_i and h_j represent the i-th and j-th historical hidden states within the sequence H, respectively.

Based on the calculated weights, the context vector c_t, which encodes key historical information, is obtained via a weighted summation:

$$c_t = \sum_{i=1}^{L} \alpha_{t,i} h_i \tag{7}$$

where: c_t denotes the context vector at prediction time t.

Finally, the context vector is fed into a fully connected layer for decoding, which outputs the predicted value of basic battery-swapping demand for the current time interval, denoted as N_p. To fully account for the uncertainty in BSS operations, a statistical analysis method is simultaneously employed to extract historical extreme scenarios. The maximum historical battery-swapping frequency for each time interval is defined as the predicted extreme demand value, denoted as N_m. This realizes a dual-demand prediction framework that balances both baseline battery-swapping demand and extreme scenarios. The structure of the LSTM-Attention model is illustrated in Fig. 2.

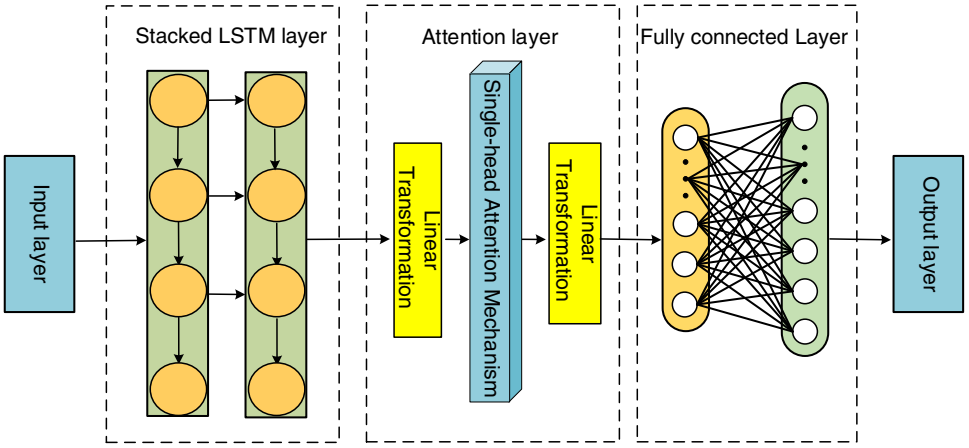

Figure 2: LSTM-Attention model architecture.

2.3 Battery Scheduling Strategy of BSS

Uncertainty in battery swap demand may lead to a mismatch between the day-ahead charging plan and the actual number of available batteries in intraday operation: when demand is low, insufficient batteries available for charging can prevent the plan from being executed; when demand is high, it can easily cause user wait times or even battery swap failures. To ensure that users have fully charged batteries available upon arrival at the station, a battery adjustment strategy needs to be introduced in addition to the day-ahead plan. Based on actual operating conditions, the battery swapping station dynamically adjusts the sequence and quantity of charging and discharging for different battery categories to cover the supply-demand gap in each period. Moreover, it is necessary to ensure that the charging and discharging plan for each period aligns as closely as possible with the day-ahead scheduling to meet swap demand. Therefore, the following battery adjustment strategy is proposed to determine the sequence and timing of battery charging and discharging.

2.3.1 Current Period Battery Dispatch Strategy

To ensure uninterrupted battery swap service, the following battery dispatch strategy is formulated for the current period. This strategy dynamically adjusts the battery status and types based on the actual battery swap demand, building upon the day-ahead forecasting output. Relevant parameter values are set as follows: SOC_{high} = 90% and SOC_{emerg} = 85% as the minimum SOC threshold for emergency battery swaps. $P_{ch,max}$ is the maximum charging power, W_B is the battery rated capacity, and t_{wait} is the maximum driver waiting time, which is set to 15 min.

Each time a battery swap demand occurs, it checks whether the current number of available fully charged Category 1 batteries N_f is greater than 0, i.e.,

$$N_f > 0 \tag{8}$$

If condition (8) is not satisfied, the emergency adjustment strategy is triggered. First, it determines whether the number of Category 2 batteries in the station satisfies:

$$N_d \geq 1 \tag{9}$$

If condition (9) is satisfied, Emergency Battery Adjustment Strategy 1 is adopted; if condition (9) is not satisfied, Emergency Battery Adjustment Strategy 2 is implemented.

(a) Battery Emergency Adjustment Strategy 1: When a battery swap demand occurs at the station but the number of Category 1 batteries is zero—meaning there are no batteries with $SOC_i \geq SOC_{high}$ available for swapping—the battery with the highest SOC among Category 2 batteries is selected and denoted as battery j, with its SOC denoted as SOC_j:

$$j = \arg\max_{i \in \Omega_d} SOC_i(t) \tag{10}$$

Its target SOC is set to SOC_{high}, and it is charged immediately at the maximum power $P_{ch,max}$. The required charging time is:

$$t_{ch,II} = \frac{(SOC_{high} - SOC_j) \times W_B}{P_{ch,max} \times 100} \tag{11}$$

The quantities of each battery category are updated as follows:

$$N_d(t)' = N_d(t) - 1 \tag{12}$$

$$N_f(t)' = N_f(t) + 1 \tag{13}$$

(b) Battery Emergency Adjustment Strategy 2: When a battery swapping demand occurs at the station but both Category 1 and Category 2 batteries are unavailable (i.e., their quantities are zero), the battery with the highest SOC among Category 3 batteries is selected and denoted as battery k, with its SOC denoted as SOC_k:

$$k = \arg\max_{i \in \Omega_c} SOC_i(t) \tag{14}$$

Its target SOC is set to SOC_{emerg}. The required charging time is calculated as:

$$t_{ch,3} = \frac{(SOC_{emerg} - SOC_k) \times W_B}{P_{ch,max} \times 100} \tag{15}$$

where: $t_{ch,3}$ denotes the total charging power of Category 3 batteries at time t.

If $t_{ch,3} \leq t_{wait}$ the battery is charged immediately at $P_{ch,max}$ until SOC_{emerg} is reached, then reclassified as a Category 1 battery and used for swapping. If $t_{ch,3} > t_{wait}$, it is determined that the swap demand cannot be met, a service failure is recorded. The quantities of each battery category are updated as follows:

$$N_c(t)' = N_c(t) - 1 \tag{16}$$

$$N_f(t)' = N_f(t) + 1 \tag{17}$$

(c) Battery Dispatch Strategy Upon Swap Completion: At the moment a battery swap is completed, check whether the number of battery swaps already performed in the current period N_h has reached the basic forecasted swap demand for this period $N_{p,this}$, i.e.,

$$N_h \leq N_{p,this} \tag{18}$$

If this condition is not satisfied, the newly depleted battery is removed from the vehicle, put into charging, its SOC target is set to SOC_{high} = 90%, and it is classified as a Category 1 battery.

2.3.2 Next Period Battery Update Strategy

(a) Battery Update Strategy 1: To ensure that the basic battery swap demand for the next period $N_{p,next}$ is met, the number of fully charged batteries remaining in the current period, combined with those being charged and converted to Category 1, must satisfy the requirement. Before the end of the current period t, ensure:

$$N_f + N_{1,ch} \geq N_{p,next} \tag{19}$$

where: $N_{1,ch}$ denotes the number of batteries already designated as Category 1 and currently under charging during this period.

If condition (19) is not satisfied, calculate the battery shortfall:

$$\Delta N_f = N_{p,next} - (N_f + N_{1,ch}) \tag{20}$$

Then select the ΔN_f batteries with the highest SOC from Category 3, charge them to convert to Category 1, and set their target SOC to SOC_{high}.

(b) Battery Update Strategy 2: To address potential extreme battery swap demand $N_{m,next}$ in the next period, ensure that the sum of the remaining fully charged batteries, Category 2 batteries, and the number of batteries undergoing charging to be converted to Category 2 in the current period satisfies the following condition before the end of period t:

$$N_f + N_d + N_{ch} \geq N_{m,next} \tag{21}$$

$$N_{ch} = N_{1,ch} + N_{2,ch} \tag{22}$$

where: $N_{2,ch}$ represents the number of batteries already designated as Category 2 and currently under charging in this period; Where N_{ch} represents the total number of batteries transitioning from the charging state to Category 1 and Category 2.

If condition (21) is not satisfied, calculate the battery shortfall:

$$\Delta N_{\mathrm{d}} = N_{\mathrm{m,next}} - \left(N_{\mathrm{f}} + N_{\mathrm{d}} + N_{\mathrm{ch}}\right) \tag{23}$$

Then select the ΔN_{d} batteries with the highest SOC from Category 3 and charge them to convert to Category 2 batteries. Their target SOC should fall within the range $\mathrm{SOC_{low}} \leq \mathrm{SOC_{target}} < \mathrm{SOC_{high}}$.

The overall battery scheduling strategy is illustrated in Fig. 3 below:

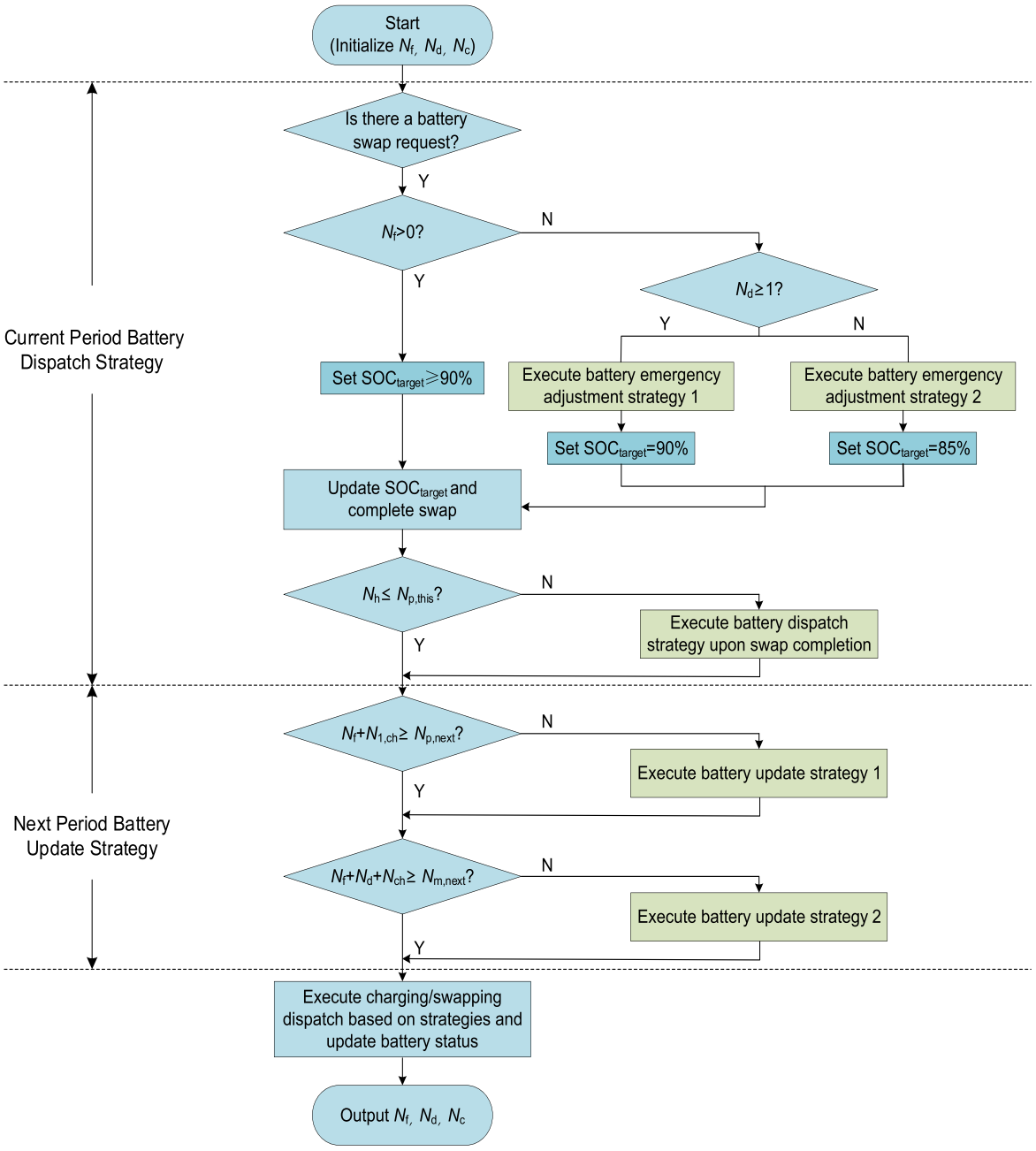

Figure 3: Battery scheduling strategy flowchart.

3 Optimization Scheduling of BSS Participating in Frequency Regulation

The overall dispatch framework for the heavy-duty truck battery swapping station assisting grid frequency regulation is illustrated in Fig. 4. It consists of a two-stage dispatch model: day-ahead scheduling based on maximizing the swap station's operational revenue and real-time adjustment considering forecast deviations. In the day-ahead stage, the grid operator formulates the next day's frequency regulation capacity requirement plan based on the overall system load fluctuations and sends it to the battery swapping station. After receiving the grid's frequency regulation plan, the heavy-duty electric truck battery swapping station, considering the in-station battery status and predicted swap demand, develops the day-ahead charging/discharging and frequency regulation capacity reservation plan with the objective of maximizing operational revenue. During the intraday operation, the swap station conducts rolling adjustments to the day-ahead scheduling results based on actual swap demand and real-time battery status, ensuring the reliability of swap services while continuously responding to the grid's regulation requirements.

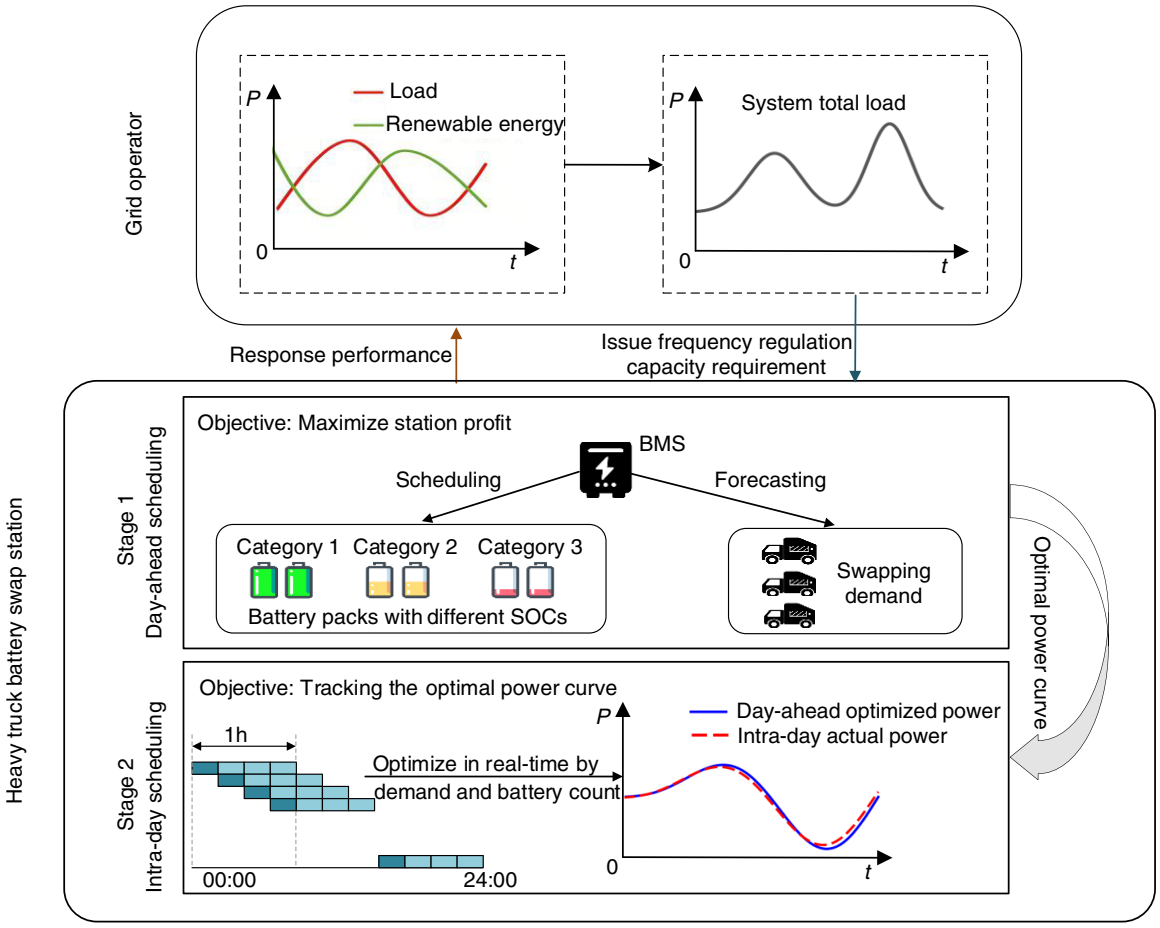

Figure 4: Overall framework diagram.

It should be pointed out that in this paper, upward and downward frequency regulation respectively represent the regulatory responses of the BSS to under-frequency and over-frequency events in the power grid. Specifically, upward frequency regulation implies that during an under-frequency event, power support is provided to the grid by the BSS through curtailing the baseline charging load or discharging the batteries. Conversely, downward frequency regulation indicates that during an over-frequency event, the capability of

absorbing active power from the grid is increased by the BSS, where surplus electrical energy is absorbed through battery charging. Furthermore, when a larger number of available batteries is present at the station, a stronger energy-absorbing capability is exhibited by the system. However, the battery power is strictly kept within its rated limits.

3.1 Day-Ahead Optimization Model

3.1.1 Objective Function

Heavy-duty truck battery swapping stations need to optimize the scheduling of the battery charging and discharging process to maximize their responsiveness to grid frequency regulation demands while ensuring user battery swap services. This aims to achieve the maximization of the station's revenue.

The objective function is to maximize the net revenue of the swap station:

$$\max F_1 = f_1 + f_2 - f_3 - f_4 \tag{24}$$

f_1 is defined as the total charges paid by EV users per swapping event, consisting of two components: the swapping service fee and the electricity consumption fee, i.e.,

$$f_1 = \sum_{t=1}^{T} \left(\alpha_{\text{swap}} R(t) + \sum_{i=1}^{R(t)} \lambda_s \left[1 - \text{SOC}_{i,t}\right] W_{\text{B}} \right) \tag{25}$$

where: α_{swap} is the fee per swap service, $R(t)$ is the actual number of battery swaps; λ_s is the retail electricity price for battery charging; $\text{SOC}_{i,t}$ is the battery state of charge of vehicle i during the battery swap in time period t; W_{B} is the rated capacity of the battery. Constant power charging is assumed.

f_2 represents the revenue from the battery swapping station's participation in auxiliary frequency regulation services. Frequency regulation revenue includes capacity revenue and mileage revenue. Capacity revenue refers to the income earned by reserving adjustable capacity for frequency regulation services, while mileage revenue refers to the income earned based on the sum of the absolute values of upward or downward power adjustments in response to frequency regulation signals:

$$f_2 = \sum_{t=1}^{T} \left(R_{\text{cap},t} + R_{\text{perf},t} \right) \tag{26}$$

$$R_{\text{cap},t} = P_{\text{cap},t} \times \lambda_{\text{cap},t} \times T \tag{27}$$

$$R_{\text{perf},t} = D_{\text{mile},t} \times \lambda_{\text{mile},t} \times K_{\text{perf},t} \tag{28}$$

where: $R_{\text{cap},t}$ is the frequency regulation capacity revenue in time period t; $R_{\text{perf},t}$ is the frequency regulation mileage revenue in time period t; $P_{\text{cap},t}$ is the awarded frequency regulation capacity bid submitted by the battery swapping station to the grid in time period t; $\lambda_{\text{cap},t}$ and $\lambda_{\text{mile},t}$ are the compensation prices for frequency regulation capacity and mileage in the frequency regulation market for time period t, respectively; $K_{\text{perf},t}$ is the frequency regulation performance coefficient; $D_{\text{mile},t}$ is the actual frequency regulation mileage completed in time period t; T is the service duration (in hours).

f_3 represents the electricity purchasing cost of the battery swapping station, i.e.,

$$f_3 = \sum_{t=1}^{T} P_{\text{BSS},t} \lambda_{\text{buy}}(t) \tag{29}$$

where: $P_{\text{BSS},t}$ is the total charging power in time period t; $\lambda_{\text{buy}}(t)$ is the electricity purchasing price.

f_4 represents the cost associated with the risk of load curtailment. To prioritize user battery swap services, this term economically quantifies the positive deviation between the forecasted demand and the actual number of available fully charged batteries using a relatively large penalty factor. This effectively mitigates the risk of battery swap failures resulting from excessive pursuit of frequency regulation revenue:

$$f_4 = \beta \sum_{t=1}^{T} \max\left(0, N_{\mathrm{P},t} - N_{1,t}\right) \tag{30}$$

where: β is the penalty coefficient; $N_{\mathrm{P},t}$ represents the forecasted basic battery swapping demand at time t; and $N_{1,t}$ represents the number of Category 1 batteries at time t.

Overall, the priority order of the aforementioned four key factors is clearly defined by the proposed model through the objective function and various constraints. First, guaranteeing the heavy-duty truck swapping demand is set as the highest priority of the system; this bottom line is not only restricted by strict physical constraints but also reflected in the penalty term formulated in Eq. (30). Second, owing to the high economic compensation provided by the auxiliary service market (Eqs. (26)–(28)), flexible batteries will be prioritized and dispatched by the optimization model to respond to grid frequency regulation, thereby maximizing the overall net revenue. Finally, the response to TOU prices is adopted as the fundamental cost-reduction measure of the system, whereby operational costs are further controlled under the premise that the preceding two high-priority tasks are satisfied.

3.1.2 Constraints

(a) Battery Quantity Constraint:

$$N = N_{\mathrm{f}}(t) + N_{\mathrm{d}}(t) + N_{\mathrm{c}}(t) \tag{31}$$

where: N represents the total number of batteries in the swap station.

(b) Charging and Discharging Power Constraints:

$$P_{\mathrm{ch}}(t) = \sum_{i \in \Omega_{\mathrm{d}}(t)} P_{\mathrm{ch},i,t} + \sum_{i \in \Omega_{\mathrm{c}}(t)} P_{\mathrm{ch},i,t} \tag{32}$$

$$P_{\mathrm{dis}}(t) = \sum_{i \in \Omega_{\mathrm{d}}(t)} P_{\mathrm{dis},i,t} \tag{33}$$

$$0 \le P_{\mathrm{ch}}(t) \le P_{\mathrm{ch,max}} \tag{34}$$

$$0 \leqslant P_{\mathrm{dis}}(t) \leqslant P_{\mathrm{dis,max}} \tag{35}$$

$$P_{\mathrm{ch}}(t) \cdot P_{\mathrm{dis}}(t) = 0 \tag{36}$$

where: $P_{\mathrm{ch},i,t}$ is the charging power of battery 1 in time period t; $P_{\mathrm{dis},i,t}$ is the discharging power of battery i in time period t; $P_{\mathrm{ch}}(t)$ and $P_{\mathrm{dis}}(t)$ are the total charging and total discharging power in time period t, respectively; $P_{\mathrm{dis,max}}$ denotes the maximum discharge power.

(c) SOC Constraint:

$$\mathrm{SOC}_{i,t+1} = \mathrm{SOC}_{i,t} + \frac{P_{\mathrm{ch},i,t}\eta_{\mathrm{ch}}\Delta t - \left(P_{\mathrm{dis},i,t}/\eta_{\mathrm{dis}}\right)\Delta t}{W_{\mathrm{B}}} \tag{37}$$

$$\mathrm{SOC}_{\min} \le \mathrm{SOC}_i \le \mathrm{SOC}_{\max}, \forall i \in N, \forall t \tag{38}$$

where: $\mathrm{SOC}_{i,t}$ denotes the state of charge of the i-th battery at time step t; η_{ch} and η_{dis} represent the constant charging and discharging efficiencies, respectively.

(d) Declared Frequency Regulation Capacity Constraints:

$$0 \le P_{\mathrm{cap},t}^{\mathrm{up}} \le \sum_{i \in \Omega_{\mathrm{d}}(t)} P_{\mathrm{dis},i,t} \tag{39}$$

$$0 \le P_{\mathrm{cap},t}^{\mathrm{down}} \le \sum_{i \in \Omega_{\mathrm{d}}(t)} P_{\mathrm{ch},i,t} + \sum_{i \in \Omega_{\mathrm{c}}(t)} P_{\mathrm{ch},i,t} \tag{40}$$

where: $P_{\mathrm{cap},t}^{\mathrm{up}}$ represents the declared upward frequency regulation capacity at time t; and $P_{\mathrm{cap},t}^{\mathrm{down}}$ represents the declared downward frequency regulation capacity at time t.

(e) Transformer Capacity Constraint:

$$P_{\mathrm{cz}}(t) \le P_{\mathrm{T,max}} \tag{41}$$

where: $P_{\mathrm{cz}}(t)$ is the total input power of the battery swapping station at time t, and $P_{\mathrm{T,max}}$ is the capacity limit of the transformer equipped at the station.

3.2 Real-Time Rolling Optimization

To enable the battery swapping station to better respond to system frequency regulation needs in real-time operation, a rolling optimization based on intraday real-time information is introduced. This paper implements real-time acquisition of updated battery swap demand information and the status of batteries at different levels through a classified battery scheduling plan. At the start of each scheduling period, based on the latest swap demand, battery status, and grid frequency regulation instructions, the charging and discharging sequence and power of batteries at each level for the current and subsequent periods are dynamically adjusted. This mechanism ensures the reliability of user battery swap demand while tracking and responding to frequency regulation capacity requirements, thereby guaranteeing the operational safety of the battery swapping station and the reliability of frequency regulation services through real-time adjustments.

3.2.1 Objective Function

The objective of the real-time phase is to mitigate power fluctuations caused by day-ahead prediction errors, ensuring that the actual operation closely tracks the day-ahead plan to reduce economic losses due to uncertainty, while also responding to the real-time AGC instructions issued by the distribution grid. The optimization model aims to minimize the deviation between the real-time output and the day-ahead plan, as well as the deviation in responding to actual frequency regulation instructions. The model is formulated as follows:

$$\min F_2 = \sum_{t=1}^{T} \left[\lambda_1 \left(P_{\mathrm{BSS},t} - P^{*}{}_{\mathrm{BSS},t} \right)^2 + \lambda_2 C_{\mathrm{fe},t} \right] \tag{42}$$

where: $P_{\mathrm{BSS},t}$ is the actual power of the battery swapping station during the intraday time period t; $P^{*}{}_{\mathrm{BSS},t}$ is the power scheduled for time period t obtained from day-ahead optimization; λ_1 and λ_2 are deviation coefficients; $C_{\mathrm{fe},t}$ is the penalty term for deviations in responding to frequency regulation instructions, expressed as:

$$C_{\mathrm{fe}.t} = \left| \sum_{i=1}^{N} \left(P_{i,t}^{\mathrm{up}} - r_t^{\mathrm{fu}} + P_{i,t}^{\mathrm{down}} - r_t^{\mathrm{fd}} \right) \right| \tag{43}$$

where: $P_{i,t}^{\mathrm{up}}$ and $P_{i,t}^{\mathrm{down}}$ are the actual upward and downward frequency regulation outputs provided by batteries; r_t^{fu} and r_t^{fd} are the real-time upward and downward frequency regulation instruction values issued by the grid.

3.2.2 Constraints

(a) Response to Frequency Regulation Signal Constraints:

When responding to AGC instructions, the battery swapping station must not exceed its maximum frequency regulation capacity while tracking the frequency regulation commands.

$$\begin{cases} 0 \le P_{i,t}^{\mathrm{up}} \le P_{i,t}^{\mathrm{up,max}},\ 0 \le P_{i,t}^{\mathrm{down}} \le P_{i,t}^{\mathrm{down,max}} \\ \sum_{i=1}^{N} P_{i,t}^{\mathrm{up}} \le r_t^{\mathrm{fu}},\ \sum_{i=1}^{N} P_{i,t}^{\mathrm{down}} \le r_t^{\mathrm{fd}} \\ P_{i,t}^{\mathrm{up}} \cdot P_{i,t}^{\mathrm{down}} = 0 \end{cases} \tag{44}$$

where: $P_{i,t}^{\mathrm{down,max}}$ and $P_{i,t}^{\mathrm{up,max}}$ denote the maximum upward and downward frequency regulation of the i-th battery at time t.

The remaining constraints remain consistent with the day-ahead constraints.

4 Solution Methodology

4.1 Linearization of Nonlinear Terms

Since the original model contains nonlinear terms, to ensure that it can be directly and optimally solved by the Gurobi solver, this paper rigorously linearizes all nonlinear terms, achieving exact equivalence with the original model. The specific transformation processes are detailed as follows:

(a) Linearization of the penalty function

In the penalty cost term of the day-ahead objective function, expressed as Eq. (30): $f_4 = \beta \sum_{t=1}^{T} \max\left(0, N_{\mathrm{P},t} - N_{1,t}\right)$, we introduce a non-negative continuous auxiliary variable $Z_t^{\mathrm{pen}} \ge 0$ to linearize it as follows:

$$f_4 = \beta \sum_{t=1}^{T} Z_t^{\mathrm{pen}} \tag{45}$$

The original nonlinear term is replaced by Z_t^{pen}, which is subject to the following linear constraint:

$$Z_t^{\mathrm{pen}} \ge N_{\mathrm{p},t} - N_{1,t} \tag{46}$$

Since the objective function aims to minimize the total cost, the solver will naturally drive Z_t^{pen} down to its tightest lower bound, exactly reflecting the value of the original max function.

(b) Linearization of the absolute value in the intraday optimization

For the intraday penalty term in Eq. (43): $C_{\mathrm{fe}.t} = \left| \sum_{i=1}^{N} \left(P_{i,t}^{\mathrm{up}} - r_t^{\mathrm{fu}} + P_{i,t}^{\mathrm{down}} - r_t^{\mathrm{fd}} \right) \right|$ used to evaluate the tracking deviation, to linearize it strictly without any approximation, we introduce a non-negative auxiliary variable $e_t \ge 0$, the tracking error is rewritten as:

$$C_{\mathrm{fe},t} = e_t \tag{47}$$

and the following linear constraints are added:

$$\begin{cases} e_t \geq \sum_{i=1}^{N} \left(P_{i,t}^{\mathrm{up}} - r_t^{\mathrm{fu}} + P_{i,t}^{\mathrm{down}} - r_t^{\mathrm{fd}} \right) \\ e_t \geq -\sum_{i=1}^{N} \left(P_{i,t}^{\mathrm{up}} - r_t^{\mathrm{fu}} + P_{i,t}^{\mathrm{down}} - r_t^{\mathrm{fd}} \right) \end{cases} \tag{48}$$

Consequently, the non-linear absolute value operation is precisely replaced by a set of equivalent linear inequalities, provided that $C_{\mathrm{fe},t}$ is being minimized in the objective function.

(c) Linearization of mutually exclusive constraints

The original Eq. (36): $P_{\mathrm{ch}}(t) \cdot P_{\mathrm{dis}}(t) = 0$ and Eq. (44): $P_{i,t}^{\mathrm{up}} \cdot P_{i,t}^{\mathrm{down}} = 0$ are both nonlinear, mutually exclusive constraints. This is because the physical states of the system dictate that a battery cannot charge and discharge simultaneously, nor can the battery swapping station provide upward and downward frequency regulation at the same time. We linearized these constraints by introducing binary indicator variables and applying the Big-M method:

For the mutually exclusive charging and discharging, a binary variable $y_t \in \{0,1\}$ is introduced to linearize $P_{\mathrm{ch}}(t) \cdot P_{\mathrm{dis}}(t) = 0$ as follows:

$$\begin{cases} P_{\mathrm{ch}}(t) \leq y_t P_{\mathrm{ch,max}} \\ P_{\mathrm{dis}}(t) \leq (1 - y_t) P_{\mathrm{dis,max}} \end{cases} \tag{49}$$

For the mutually exclusive upward and downward frequency regulation capacities, a binary variable $u_{i,t} \in \{0,1\}$ is introduced to linearize $P_{i,t}^{\mathrm{up}} \cdot P_{i,t}^{\mathrm{down}} = 0$ as follows:

$$\begin{cases} P_{\mathrm{i,t}}^{\mathrm{up}} \leq u_{i,t} P_{\mathrm{i,t}}^{\mathrm{up,max}} \\ P_{i,t}^{\mathrm{down}} \leq (1 - u_{i,t}) P_{i,t}^{\mathrm{down,max}} \end{cases} \tag{50}$$

4.2 Solution Procedure

The proposed two-stage optimal scheduling strategy for the EHDT-BSS involves nonlinear constraints and strong coupling across multiple time scales. To enhance computational tractability and solution efficiency, a hierarchical solution framework integrating day-ahead global optimization and real-time rolling adjustment is developed. The detailed solution procedure is described as follows:

In the day-ahead stage, the scheduling horizon is set to 24 h with an hourly time resolution. Based on the forecasted battery swapping demand and time-of-use electricity prices, the optimization problem is formulated as a mixed-integer linear programming (MILP) model. By solving this model, the optimal charging and discharging schedules of battery packs for each time period, as well as the corresponding frequency regulation capacity to be submitted, are determined. The resulting solution is treated as the baseline dispatch plan for the subsequent real-time operation.

In the real-time stage, a rolling optimization strategy based on model predictive control (MPC) is adopted. With a one-period rolling horizon, the baseline day-ahead schedule is dynamically adjusted according to the realized battery swapping demand and real-time grid frequency regulation signals. This rolling correction mechanism effectively mitigates the adverse economic impacts caused by forecasting errors and improves the operational robustness of the EHDT-BSS.

All simulations are implemented on a Python 3.8 platform, and the proposed optimization models are solved using the Gurobi 9.5 solver.

5 Case Study

5.1 Basic Parameters

The relevant parameters of an actual EHDT-BSS in Deyang City, Sichuan Province, are adopted in this paper as a case study for strategy verification. Approximately 60 EHDTs are served by this swapping station, and these vehicles are assumed to be equipped with identical battery packs. To forecast the battery swapping demand, actual historical swapping order data collected over three consecutive months from this station is utilized. The relevant parameters of the swap station are set as shown in Table 1 below:

Table 1: Parameter settings.

Parameter	Value
Number of chargers	8
Number of spare batteries	8
Battery rated capacity (kWh)	280
Rated charge/discharge power (kW)	280
Maximum charge/discharge power (kW)	480
Charge/discharge efficiency	0.95
Swapping service fee (CNY/service)	80
Swapping electricity price (CNY/kWh)	1.0

The time-of-use (TOU) electricity data are shown in Table 2.

Table 2: TOU electricity prices.

Period Type	Time Slot	Price (CNY/kWh)
Peak Period	10:00–15:00, 18:00–21:00	0.8444
Flat Period	07:00–10:00, 15:00–18:00, 21:00–23:00	0.6397
Valley Period	00:00–07:00, 23:00–24:00	0.4430

5.2 Battery Swapping Demand Forecasting Results

Based on three consecutive months of historical battery swap order data from the station, an LSTM-Attention model was constructed and trained to predict the battery swap demand for the 24-time intervals of the following day. Fig. 5 shows a comparison between the actual number of swaps and the model predictions for a typical day. It can be observed that the intraday swap demand exhibits a clear bimodal distribution. Driven by the operating patterns of heavy-duty trucks, swapping activities are highly concentrated in the early morning and afternoon [25–27], with peaks occurring between 3–6 h and 13–17 h. The model can capture the trend and timing of the peak periods fairly accurately, although it slightly underestimates the peak magnitudes, and some peaks appear somewhat smoothed. Predictions during off-peak periods are generally consistent with the actual values, without producing significant false high-demand events, indicating the model's strong ability to track intraday trends.

To validate the effectiveness of the adopted approach, a comparative analysis was conducted using a standard LSTM model as a baseline. From the model evaluation metrics in Table 3, the coefficient of determination (R^2) of the proposed Stacked LSTM-Attention (ATT-SLSTM) model is 0.7880, outperforming the standard LSTM model (0.7425). This indicates that the proposed model can more effectively explain the

overall intraday fluctuations in battery swapping demand at the station. Furthermore, the mean absolute error (MAE), root mean square error (RMSE), and mean squared error (MSE) of our model are 0.7083, 0.8898, and 0.7917, respectively. These error metrics are significantly lower than those of the standard LSTM baseline (MAE = 0.8135, RMSE = 1.0425, MSE = 1.0868). Although the RMSE metric obtained by the Stacked LSTM-Attention model is slightly higher than its MAE value, reflecting some remaining prediction deviation during peak battery-swapping periods, the comparison results clearly demonstrate that incorporating the attention mechanism significantly enhances the model's ability to focus on critical historical time steps, thereby substantially reducing prediction errors. Overall, the adopted model can effectively identify peak swapping demand and intraday variation patterns for heavy-duty trucks, providing a sufficiently reliable prediction input to support the subsequent battery scheduling at the swapping station.

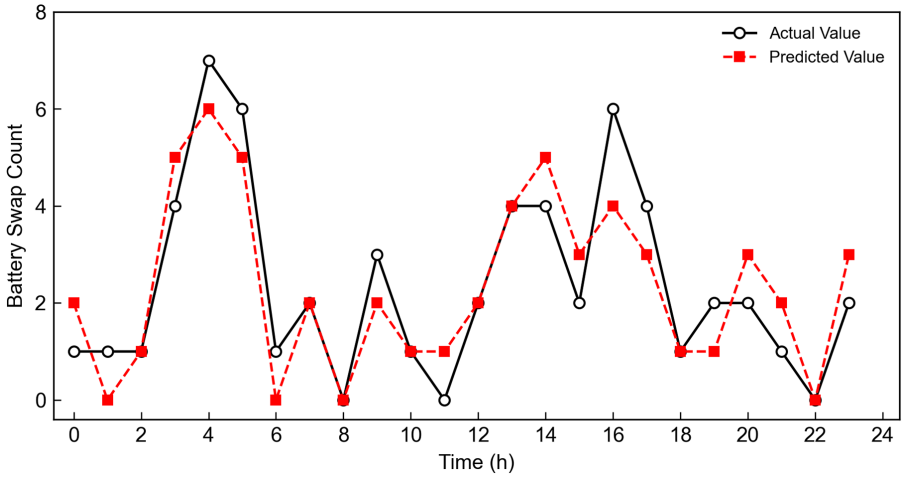

Figure 5: Prediction results of the LSTM-Attention model.

Table 3: Model performance evaluation metrics.

Metric	LSTM	ATT-SLSTM
R^2	0.7425	0.7880
MAE	0.813	0.7083
RMSE	1.0425	0.8898
MSE	1.0868	0.7917

5.3 Two-Stage Optimal Scheduling Results

5.3.1 Results and Analysis of the Day-Ahead Optimization Strategy

The frequency regulation capacity declared by the BSS is shown in Fig. 6. The figure shows the declared upward and downward regulation capacities in each time period and their relationship with the battery swapping demand. As can be observed from Fig. 6, the declared upward and downward regulation capacities of the BSS exhibit a clear negative correlation with battery swapping demand. The overall trend indicates that higher battery swapping demand corresponds to lower declared frequency regulation capacity. Conversely, when battery swapping demand is low, a higher regulation capacity is declared to increase revenue from frequency regulation services. For example, during time periods 3 and 4, the swapping demand reaches the daily peak, and the corresponding declared regulation capacities in these two periods are extremely low. During time periods 6 to 11, the swapping demand remains at a relatively low level, and thus the

declared regulation capacity stays at a high level. These results verify the flexibility of the proposed day-ahead optimization strategy, which ensures swapping service reliability while increasing economic benefits by allocating more regulation capacity during low-demand periods.

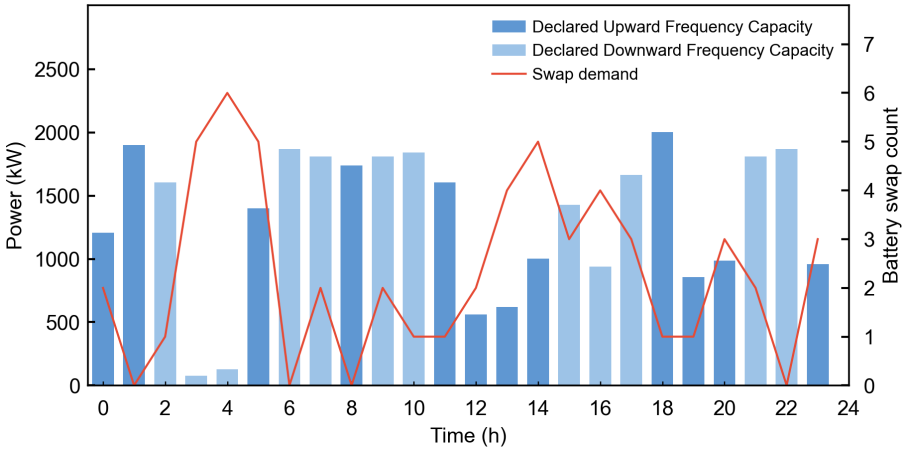

Figure 6: Declared frequency regulation capacity.

Fig. 7 shows the baseline charging schedule of the BSS under multiple constraints, which exhibits a clear stepwise pattern. The system responds to TOU electricity prices by charging at high power during off-peak periods. For instance, the charging power increases significantly during periods 2–5 and reaches its daily peak at 05:00, effectively utilizing low-cost electricity and preparing sufficient energy for the morning swapping demand peak. In contrast, charging power is reduced during high-price periods, such as 9–10 and 21–22, to lower electricity costs. However, the charging strategy is not solely driven by price signals, as it is also constrained by swapping demand and frequency regulation requirements. During high-demand periods, the system performs advanced charging even at higher prices to avoid service interruption penalties, highlighting the trade-off between reliability and economic efficiency. Moreover, the baseline power reserves adequate flexibility for real-time AGC response, enabling coordinated optimization of electricity price arbitrage and ancillary service provision.

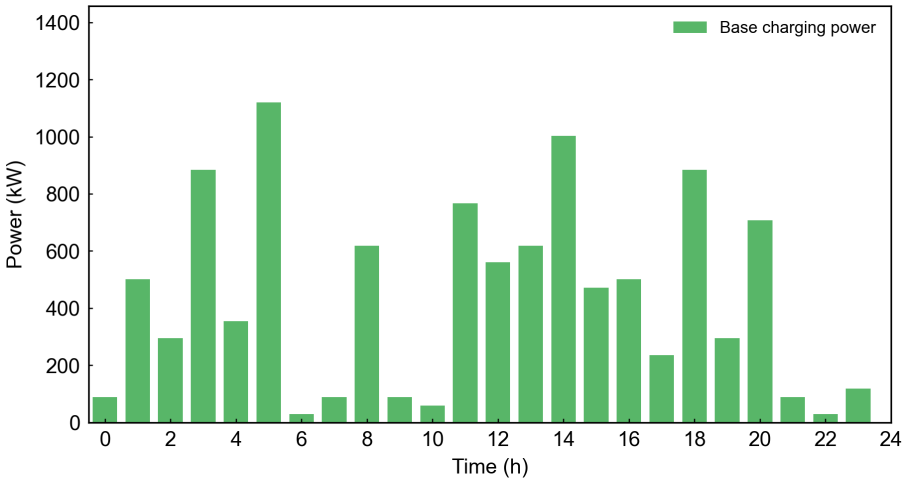

Figure 7: Baseline charging power of the BSS.

Fig. 8 illustrates the overall operational profiles of the battery swapping station. Fig. 8a presents the total equivalent charging and discharging power of the station, while Fig. 8b shows the average SOC of the station at the initial time step. In Fig. 8a, the green bars represent the maximum charging power that can be provided by the station in each period. It should be noted that the red bars do not indicate continuous net discharging power; instead, they represent the maximum equivalent discharging power reserved by the station. This capacity comprises the actual power injected into the grid and the reduction in scheduled charging power. In practice, the regulation is primarily achieved by reducing the baseline charging power, and only when the required regulation exceeds the total scheduled charging power in a given period is short-term reverse discharging of batteries additionally employed. Overall, the charging load is shifted forward to low electricity price periods or delayed to flat-price periods along the time dimension, thereby avoiding operation during peak price periods and reducing cost pressure. Meanwhile, this flexibility enables valuable downward frequency regulation capacity to be provided to the grid. For example, during peak price periods (11:00–14:00 and 18:00–20:00), charging behaviors are shifted forward or delayed, which effectively contributes to system stability by providing downward regulation capacity.

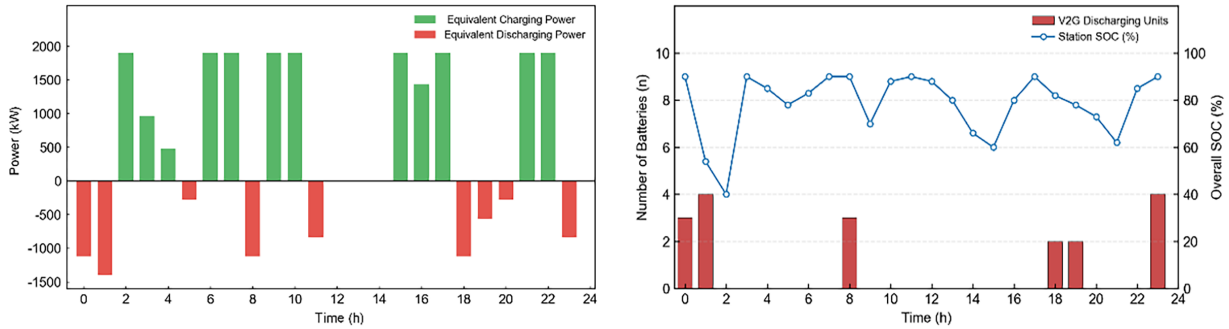

Figure 8: Operation profile of the BSS.

Fig. 8b presents the overall SOC profile of the station along with the number of batteries reserved for participation in discharging. To prioritize the battery swapping demand of heavy-duty trucks, only a limited number of batteries are scheduled to participate in V2G discharging. Throughout the day, the station's overall SOC is maintained within the range of 40%–90%. During peak swapping periods (e.g., Periods 3 and 4), a high SOC is maintained, and no frequency regulation discharging service is provided. In contrast, during low swapping demand periods when upward regulation is required by the grid (e.g., Periods 18 and 19), support is provided through reduced charging power and limited short-term battery discharging, during which the overall SOC decreases but remains above 50%. In general, the optimized strategy effectively shifts the charging load to non-peak electricity price periods, thereby reducing operational costs while simultaneously ensuring both the battery swapping demand for heavy-duty trucks and reliable frequency regulation support for the grid.

As shown in Table 4, the revenues of the battery swapping station before and after optimization are compared. In the day-ahead optimized scenario, the station obtains 4278.35 CNY from frequency regulation services. Although electricity purchasing costs increase, the ancillary service revenue offsets the additional cost, resulting in a net profit of 8960.75 CNY. In contrast, the non-optimized scenario has lower charging costs (3971.45 CNY) but no regulation revenue, leading to lower overall profit. These results indicate that the proposed frequency regulation participation strategy can significantly improve the economic performance of the battery swapping station.

Table 4: Comparative analysis of the unoptimized scenario and day-ahead optimization results.

Scenario	Electricity Procurement Cost (CNY)	Regulation Capacity Revenue (CNY)	Regulation Mileage Revenue (CNY)	Swapping Service Revenue (CNY)	Net Profit (CNY)
Unoptimized	3971.45	0	0	10,368.00	6396.55
Day-ahead	5685.60	1109.15	3169.20	10,368.00	8960.75

To verify the economic adaptability of the proposed framework, a sensitivity analysis on regulation prices is conducted in this section. With other parameters kept constant, the baseline prices (0.035 CNY/kW for regulation capacity and 0.05 CNY/kW for mileage) are scaled by ±40%, respectively. The results are summarized in Table 5.

Table 5: Revenue comparison under different frequency regulation service prices.

Regulation Capacity Price (CNY/kW)	Regulation Mileage Price (CNY/kW)	Electricity Procurement Cost (CNY)	Regulation Capacity Revenue (CNY)	Regulation Mileage Revenue (CNY)	Swapping Service Revenue (CNY)	Net Profit (CNY)
0.021	0.030	5515.03	643.67	1916.29	10,368.00	7412.93
0.035	0.05	5685.60	1109.15	3169.20	10,368.00	8960.75
0.049	0.070	5827.74	1739.15	4968.91	10,368.00	11,248.32

The data indicate that price signals are effectively responded to by the proposed model. As regulation compensation increases, the scheduling priority is tilted toward ancillary services. In the scenario with higher regulation prices, although the procurement cost slightly rises to 5827.74 CNY due to the enhancement of regulation capacity, the total profit increases by approximately 25.5%. Conversely, when the regulation prices decrease, the declared capacity is reduced by the model to focus on minimizing procurement costs via peak-valley price differentials. Throughout all scenarios, the swapping service revenue remains constant, validating the strategy's capability in prioritizing swapping demand while flexibly allocating resources and synergistically optimizing multi-objective revenues.

5.3.2 Results and Analysis of the Intra-Day Optimization Strategy

Due to the uncertainty of user swapping demand, although day-ahead forecasting is performed, there are inevitable deviations between the actual number of battery swaps and the predicted results. In addition, the real-time AGC signals issued by the grid may also differ from the day-ahead AGC signals. Therefore, intraday real-time adjustments are required. Through the battery scheduling strategy and intraday optimization, the charging and discharging power of the station's battery system is adjusted to rapidly respond to AGC signals while ensuring user swapping demand, thereby ensuring close consistency between the regulation market response and the actual AGC commands.

As shown in Fig. 9, the battery swapping station is able to effectively track the AGC signal during most periods, with the actual regulation power closely following the command curve, demonstrating good dynamic response and tracking performance. However, during the period of 18:00–19:00, the regulation output decreases to a certain extent, leading to deviations in responding to upward regulation commands.

This is mainly due to the significantly increased swapping demand during 16:00–17:00, which reduces the available battery resources for frequency regulation as the system prioritizes the reliability of swapping services, thereby limiting the regulation capability in subsequent periods. This phenomenon indicates a trade-off between battery swapping service provision and frequency regulation performance, while also demonstrating the adaptability of the proposed strategy in dynamically allocating battery resources under different operating conditions.

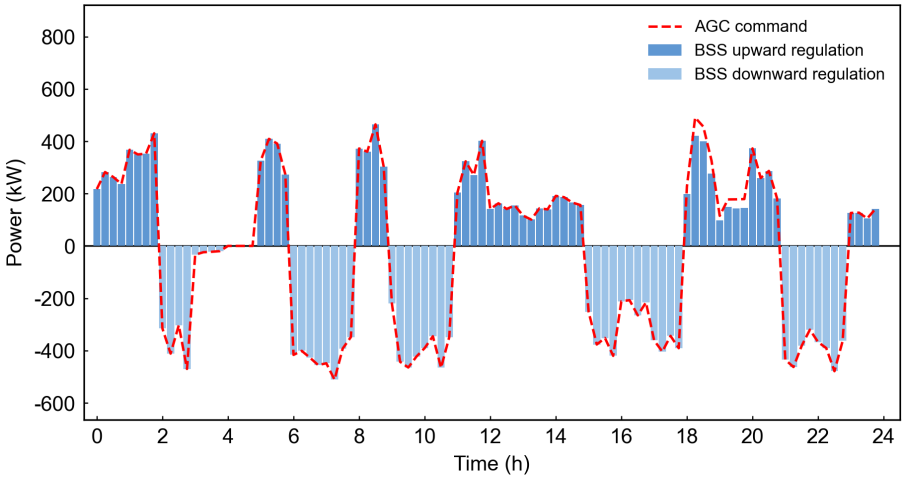

Figure 9: Real-time response of the battery swapping station to AGC signals.

Table 6 presents a comparison of the revenue results of the battery swapping station after day-ahead and intraday optimization. It can be observed that the net profit in the intraday stage is 8223.46 CNY, which is only reduced by 8.23% compared with the day-ahead plan but increased by 28.56% compared with the unoptimized system. This verifies the economic stability of the proposed model in real-time operation. Due to the uncertainty of user swapping behavior, the intraday adjustment strategy prioritizes swapping service reliability by reducing real-time frequency regulation capacity, resulting in a decrease in total regulation revenue to 3796.98 CNY and the introduction of certain penalty costs. However, this strategy successfully avoids the risk of energy replenishment shortages caused by a sudden increase in vehicle arrivals, and the overall revenue of the battery swapping station remains considerable.

Table 6: Comparison between day-ahead scheduling plan and intra-day operational results.

Scenario	Electricity Procurement Cost (CNY)	Regulation Capacity Revenue (CNY)	Regulation Mileage Revenue (CNY)	Swapping Service Revenue (CNY)	Penalty (CNY)	Net Profit (CNY)
Day-ahead	5685.60	1109.15	3169.20	10,368.00	0	8960.75
Intra-day	5913.02	998.24	2798.74	10,560.00	220.50	8223.46

5.4 Potential Impacts and Sensitivity Discussion of Battery Degradation

The increased charging and discharging operations for providing grid frequency regulation services may accelerate battery degradation, which in turn affects the long-term economics of the EHDT-BSS. This study did not explicitly incorporate battery degradation costs into the objective function, aiming to focus

on validating the effectiveness of the proposed two-stage optimal scheduling strategy while maintaining the model's computational efficiency. Nevertheless, this section provides a quantitative and qualitative analysis of the potential impacts of battery degradation, combining battery life characteristics with economic sensitivity.

According to the GB/T 31484-2015 standard, a traction battery is considered to have reached its end-of-life threshold when its discharge capacity degrades to 80% of the initial rated capacity. The lithium iron phosphate batteries widely used in current EHDTs typically have a standard cycle life of 3500 to 5000 equivalent full cycles. In the scheduling strategy proposed in this paper, the SOC is strictly limited within a safe operating range of 30% to 90%. This effectively avoids irreversible damage such as deep over-discharging at low SOC levels and overcharge-induced lithium plating at high SOC levels. Based on calculations, the equivalent full cycles of the batteries under this strategy are approximately 400–500 times per year. The converted service life until reaching 80% of the rated capacity is about 5 to 8 years, which is basically consistent with the natural calendar life of the batteries.

Economically, existing studies have confirmed that battery degradation under scientific scheduling is controllable, and the additional revenue generated from grid ancillary services is sufficient to offset the annualized battery amortization costs caused by the increased charging and discharging frequency [28]. Therefore, under the premise of reasonable SOC boundary management, the strategy proposed in this paper possesses strong engineering practical value. Future work will explore introducing a linearized energy-throughput-based degradation cost into the model framework to achieve a comprehensive co-optimization of battery life and operational revenue.

6 Conclusion

This paper establishes a two-stage optimal scheduling model for electric heavy-duty truck battery swapping stations participating in grid frequency regulation and proposes a coordinated operation strategy considering the uncertainty of battery swapping demand. Based on comparative simulation analysis, the following conclusions are drawn.

(1) The SOC-based battery classification method and scheduling strategy can effectively integrate the internal battery resources of the swapping station. While ensuring the reliability of heavy-duty truck battery swapping services, the station can rapidly respond to AGC frequency regulation signals, fully utilizing its flexibility potential as a regulation resource. This enables the coordinated operation of swapping services and ancillary services and improves the economic benefits of the swapping station by participating in the frequency regulation service.

(2) A coupling relationship exists between battery swapping demand and frequency regulation capacity. By optimizing the declaration of regulation capacity and the allocation of charging and discharging power, the swapping station can dynamically release its regulation capability while guaranteeing service reliability, thereby improving the tracking accuracy of AGC signals and frequency regulation performance, and enhancing the operational stability of the power grid.

(3) The proposed two-stage optimal scheduling framework can effectively improve the benefits of the swapping station and mitigate deviations between the day-ahead optimal results and real-time operation. This ensures consistency between actual operation and the day-ahead optimal plan, and improves the economic performance and robustness of the scheduling strategy under uncertain operating conditions.

In summary, the proposed two-stage optimization framework based on SOC classification demonstrates strong scalability and engineering application feasibility. Through rigorous linearization, the model maintains high computational efficiency even when scaled up to larger BSS scenarios. Simultaneously,

the highly compatible SOC-based classification mechanism can flexibly accommodate complex real-world operating conditions—such as battery heterogeneity and time-varying charging power—without altering the core architecture. However, this study has certain limitations: the current model does not explicitly incorporate non-linear battery degradation costs into the objective function, which somewhat simplifies the long-term economic assessment of the system. Additionally, certain simplifications were made regarding battery heterogeneity and charging power limits. Therefore, future research could introduce a linearized energy-throughput-based degradation cost into the modeling framework. By incorporating SOC-dependent dynamic power boundaries and integrating battery SOH assessment indicators, future work will further refine battery classification and boundary constraints, thereby enhancing the practical value and robustness of the proposed strategy in complex and dynamic grid environments.

Acknowledgement: All authors express gratitude for the support and cooperation provided by their respective institutions.

Funding Statement: This research was supported by Science and Technology Project of State Grid Sichuan Electric Power Company, titled "Research on Market Mechanisms and Operational Strategies for Vehicle-Grid Interaction Adapted to Spatiotemporal Supply-Demand Balance Needs in Sichuan" (No. 52199925000M).

Author Contributions: Xin Li: Conceptualization, Methodology, Formal analysis, Software development; Shuang Shi: Data curation, Validation, Review and editing; Qiyi Liu: Formal analysis, Software development; Yan Zhang: Data curation, Validation. All authors reviewed and approved the final version of the manuscript.

Availability of Data and Materials: All data generated or analyzed during this study are included in this published article.

Ethics Approval: This study did not involve human participants or animals, and therefore ethical approval was not required.

Conflicts of Interest: The authors declare no conflicts of interest.

References

1. Zhong Z, Chen Y, Fu M, Li M, Yang K, Zeng L, et al. Role of CO_2 geological storage in China's pledge to carbon peak by 2030 and carbon neutrality by 2060. Energy. 2023;272(1):127165. doi:10.1016/j.energy.2023.127165.
2. International Energy Agency. Global EV outlook 2024. Paris, France: IEA; 2024.
3. Cao X, Jin C, Liu Y, Guo P, Qu Z. Research on capacity optimization configuration of modular battery swap stations for electric heavy-duty trucks in railway construction scenarios. In: Proceedings of the 2024 Boao New Power System International Forum—Power System and New Energy Technology Innovation Forum (NPSIF); 2024 Dec 8–10; Qionghai, China. p. 651–6.
4. Wu H. A survey of battery swapping stations for electric vehicles: operation modes and decision scenarios. IEEE Trans Intell Transp Syst. 2022;23(8):10163–85. doi:10.1109/TITS.2021.3125861.
5. Alhazmi YA. Electric vehicle battery swap stations: an overview and critical review. J Umm Al Qura Univ Eng Archit. 2025. doi:10.1007/s43995-025-00215-z.
6. Mohanty PK, Pradhan R, Jena P, Padhy NP. Renewable energy-based EV battery swapping stations: opportunities and future directions. In: Hybrid renewable power infrastructure for sustainable electric vehicle development. Singapore: Springer Nature Singapore; 2025. p. 141–68.
7. Yang H, Guo C, Ren J, Sheng J. A coordinated charging strategy on battery swapping station in microgrid considering battery to grid. In: Proceedings of the 2019 IEEE Innovative Smart Grid Technologies-Asia (ISGT Asia); 2019 May 21–24; Chengdu, China. p. 3322–6.
8. Wu X, Liu P, Lu X. Study on operating cost economy of battery-swapping heavy-duty truck in China. World Electr Veh J. 2021;12(3):144. doi:10.3390/wevj12030144.

9. Wang R, Martinez A, Allybokus Z, Zeng W, Obrecht N, Moura S. Electrifying heavy-duty trucks: battery-swapping versus fast charging. IEEE Trans Smart Grid. 2025;16(5):3989–4003. doi:10.1109/TSG.2025.3571819.
10. Çabukoglu E, Georges G, Küng L, Pareschi G, Boulouchos K. Battery electric propulsion: an option for heavy-duty vehicles? Results from a Swiss case-study. Transp Res Part C Emerg Technol. 2018;88(5):107–23. doi:10.1016/j.trc.2018.01.013.
11. Shi P, Ni G, Jin R, Wang H, Wang J, Sun Z, et al. Multi-timescale battery-charging optimization for electric heavy-duty truck battery-swapping stations, considering source–load–storage uncertainty. Energies. 2025;18(2):241. doi:10.3390/en18020241.
12. Song C, Huang Y, Xu J, Deng X. Optimal scheduling model of battery swapping station with virtual power plant mode. In: Proceedings of the 2024 IEEE 4th International Conference on Power, Electronics and Computer Applications (ICPECA); 2024 Jan 26–28; Shenyang, China. p. 648–55.
13. Choi DI, Lim DE. Analysis of the state-dependent queueing model and its application to battery swapping and charging stations. Sustainability. 2020;12(6):2343. doi:10.3390/su12062343.
14. Wang FY, Chen Z, Hu Z. Comprehensive optimization of electrical heavy-duty truck battery swap stations with a SOC-dependent charge scheduling method. Energy. 2024;308(4):132773. doi:10.1016/j.energy.2024.132773.
15. Su X, Li W, Li X. Research on ordered charging of battery swapping station based on adaptive genetic algorithm. In: Proceedings of the 2019 IEEE Sustainable Power and Energy Conference (iSPEC); 2019 Nov 21–23; Beijing, China. p. 792–6.
16. Wu H, Pang GK, Choy KL, Lam HY. A charging-scheme decision model for electric vehicle battery swapping station using varied population evolutionary algorithms. Appl Soft Comput. 2017;61(2):905–20. doi:10.1016/j.asoc.2017.09.008.
17. Tang M, Zhang C, Zhang Y, Yan Y, Wang W, An B. A dual-layer MPC of coordinated control of battery load demand and grid-side supply matching at electric vehicle swapping stations. Energies. 2024;17(4):879. doi:10.3390/en17040879.
18. Hu L, Yue F. Research on intelligent peak-cutting and valley-filling charging and swapping mode based on potential game theory. J Phys Conf Ser. 2022;2189(1):012013.
19. Feng J, Hou S, Yu L, Dimov N, Zheng P, Wang C. Optimization of photovoltaic battery swapping station based on weather/traffic forecasts and speed variable charging. Appl Energy. 2020;264:114708. doi:10.1016/j.apenergy.2020.114708.
20. Revankar SR, Kalkhambkar VN. Grid integration of battery swapping station: a review. J Energy Storage. 2021;41(4):102937. doi:10.1016/j.est.2021.102937.
21. Wang Z, Hou S. Optimal participation of battery swapping stations in frequency regulation market considering uncertainty. Energy. 2024;302:131815. doi:10.1016/j.energy.2024.131815.
22. Wang X, Wang J, Liu J. Vehicle to grid frequency regulation capacity optimal scheduling for battery swapping station using deep Q-network. IEEE Trans Ind Inform. 2021;17(2):1342–51. doi:10.1109/TII.2020.2993858.
23. Yang N, Zhao X, Li J, Wang J, Jiang H, Zhang S. Secondary frequency regulation strategy for battery swapping stations considering the behavioral model of electric vehicles. Electronics. 2025;14(8):1598. doi:10.3390/electronics14081598.
24. Romdlony MZ, Khayr RA, Muharam A, Priandana ER, Sasmono S, Rosa MR, et al. LSTM-based forecasting on electric vehicles battery swapping demand: addressing infrastructure challenge in Indonesia. J Mechatron Electr Power Veh Technol. 2023;14(1):72–9. doi:10.14203/j.mev.2023.v14.72-79.
25. Wang Z. Battery-swapping battery electric vehicles. In: Annual report on the big data of new energy vehicle in China (2023). Singapore: Springer Nature Singapore; 2024. p. 211–53.
26. Walz K, Rudion K. Charging profile modeling of electric trucks at logistics centers. Energies. 2024;17(22):5613. doi:10.3390/en17225613.
27. Song S, Qiu Y, Coates R, Dobbelaere C, Seles P. Depot charging schedule optimization for medium- and heavy-duty battery-electric trucks. World Electr Veh J. 2024;15(8):379. doi:10.3390/wevj15080379.
28. Calearo L, Marinelli M. Profitability of frequency regulation by electric vehicles in Denmark and Japan considering battery degradation costs. World Electr Veh J. 2020;11(3):48. doi:10.3390/wevj11030048.